Crystal Size Distribution (CSD) as a proxy of granitoid magmatic processes in southern Mexico

Distribución del tamaño de cristales (CSD) como indicador de los procesos magmáticos de granitoides en el Sur de México

María del Sol **Hernández-Bernal**[1,*], Pedro **Corona-Chávez**[2], Guillermo **Suazo-Cruz**[3], Elesbaan **Reséndiz-Zarco**[3], Ninfa Lizbeth **Romero-Carrillo**[4], Stefano **Poli**[5]

[1] Escuela Nacional de Estudios Superiores, Unidad Morelia, Universidad Nacional Autónoma de México, Antigua Carretera a Pátzcuaro 8701, S/N, Indeco la Huerta, 58190, Morelia, Michoacán, México.

[2] Instituto de Investigaciones en Ciencias de la Tierra, Universidad Michoacana de San Nicolás de Hidalgo, Avenida Francisco J. Múgica S/N, Edificio U-3, Ciudad Universitaria, 58030, Morelia, Michoacán, México.

[3] Maestría en Geociencias y Planificación del Territorio, Universidad Michoacana de San Nicolás de Hidalgo, Avenida Francisco J. Múgica S/N, Edificio U-3, Ciudad Universitaria, 58030, Morelia, Michoacán, México.

[4] Facultad de Ciencias de la Tierra, Universidad Autónoma de Nuevo León, Carretera a Cerro Prieto Km 8, Ejido Ex-hacienda de Guadalupe, 67700 Linares, Nuevo León, México.

[5] Dipartimento di Scienze della Terra, Università degli Studi di Milano, Via Sandro Botticelli, 23, 20133, Milano, Italy.

* Corresponding author: (M.S. Hernández-Bernal) *msol_hernandez@enesmorelia.unam.mx*

How to cite this article:
Hernández-Bernal, M.S., Corona-Chávez, P., Suazo-Cruz, G., Reséndiz-Zarco, E., Romero-Carrillo, N.L., Poli, S., 2025, Crystal Size Distribution (CSD) as a proxy of granitoid magmatic processes in southern Mexico: Boletín de la Sociedad Geológica Mexicana, 77(2), A120325. http://dx.doi.org/10.18268/BSGM2025v77n2a120325

Manuscript received: February 2, 2025
Corrected manuscript received: February 28, 2025
Manuscript accepted: March 3, 2025

Peer Reviewing under the responsibility of Universidad Nacional Autónoma de México.

ABSTRACT

Magmatic differentiation is a key process behind the diversity of continental crust rocks. Crystal Size Distribution (CSD) is a stereological-textural method that provides insights into nucleation and crystal growth, especially when integrated with geochemical and petrological data. While most CSD studies focus on igneous textures in volcanic rocks, particularly in K-feldspar and plagioclase crystals, fewer address granitoid textures. This study presents CSD analyses of eight plutonic bodies from Michoacán, southern Mexico, supported by geochemical, chronological, and thermobarometric data. These granitoids range in composition from tonalite to granite and display calc-alkaline arc signatures in major and trace elements. U-Pb zircon ages span from the Jurassic to the Miocene (164.8-20.6 Ma), suggesting long-term magmatic activity. CSD plots of plagioclase crystals indicate open magmatic systems with variable conditions, inconsistent with simple cooling. Granitoids hosting mafic microgranular enclaves show concave-up CSD trends and abrupt slope changes, implying magma mixing. Estimated average residence times (τ) range from 17 to 67 years for crystals <0.5 mm and 86 to 187 years for larger crystals (>0.5 mm), aligning with theoretical diffusion times during magma mixing and assimilation in intermediate to silicic systems. Combined CSD and thermobarometric data propose an inverse relationship between magma temperature, silica content, and crystal residence time at shallow emplacement levels. These findings provide new insights into the dynamics of crustal magma chambers and the physical parameters influencing pluton emplacement in arc-related settings.

Keywords: Crystal Size Distribution, Residence Times, Magmatic Processes, Magmatic arc, southern México.

RESUMEN

La diferenciación magmática es un proceso clave en la diversidad de las rocas de la corteza continental. La Distribución del Tamaño de Cristales (CSD, por sus siglas en inglés) es un método estereológico-textural que permite entender las etapas de nucleación y crecimiento cristalino, especialmente cuando se integra con datos geoquímicos y petrológicos. Aunque la mayoría de los estudios de CSD se enfocan en texturas ígneas de rocas volcánicas, en particular en cristales de feldespato potásico y plagioclasa, son escasos los trabajos que analizan texturas en rocas graníticas. Este estudio presenta análisis de CSD de ocho cuerpos plutónicos del estado de Michoacán, en el sur de México, apoyados en datos geoquímicos, cronológicos y termobarométricos. Estos granitoides varían en composición desde tonalitas hasta granitos y muestran firmas típicas de arcos magmáticos calcialcalinos, según sus contenidos de elementos mayores y traza. Las edades U-Pb en zircón, nuevas y compiladas, abarcan desde el Jurásico hasta el Mioceno (164.8-20.6 Ma), lo que sugiere una actividad magmática prolongada. Los diagramas CSD de plagioclasa indican sistemas magmáticos abiertos con condiciones variables, incompatibles con un enfriamiento simple. Los granitoides que contienen enclaves máficos microgranulares muestran tendencias cóncavas hacia arriba y cambios abruptos en la pendiente, lo que sugiere procesos de mezcla de magmas. El tiempo promedio de residencia (τ) estimado varía entre 17 y 67 años para cristales menores de 0.5 mm y entre 86 y 187 años para cristales mayores; tiempos comparables con los teóricos de difusión durante procesos de mezcla y asimilación en sistemas intermedios a félsicos. Los datos combinados de CSD y termobarometría proponen una relación inversa entre la temperatura del magma, el contenido de sílice y el tiempo de residencia de los cristales, en condiciones de emplazamiento somero. Estos resultados ofrecen nuevas perspectivas sobre la dinámica de las cámaras magmáticas corticales.

Palabras clave: Distribución del Tamaño de Cristales, Tiempos de Residencia, Procesos Magmáticos, Arco Magmático, sur de México.

http://dx.doi.org/10.18268/BSGM2025v77n2a120325

1. Introduction

Continental crust growth and igneous rocks diversity are closely related to magmatic differentiation processes. The composition of magma evolves in proportion to the physical and chemical changes caused by the nucleation and growth of crystals and their following fractionation (Marsh, 2013). Comprehensive igneous rock textures analysis is essential to interpret magma chamber fluid dynamics and chemical processes within it, and its thermal history (Bryon *et al.*, 1995).

Nucleation and crystal growth processes initiate the separation phase in a system that has become supersaturated (Aspillaga *et al.*, 2023; Teran *et al.*, 2010). Crystallization and the resulting solid fraction significantly influence magma rheology, as well as the mechanisms of segregation, ascent, and emplacement through the crust (Babazadeh *et al.*, 2021). Crystal growth is essentially a time-dependent process (Avrami, 1939; Marsh, 1998). The crystallization of bulk magma can be characterized by typical nucleation (J_0) and growth (G_0) rates, associated with a characteristic crystallization time (τ) (Jerram and Martin, 2008).

Given a timescale set by cooling, nucleation and growth are straightforwardly locally adjusted to achieve full crystallinity. This is especially so for intrusive rocks. That is, most of the completely crystalline igneous rocks are concerned with the cooling regime (Marsh, 1998). In plutons, the regular crystal size is proportional to the total cooling time. Small bodies have small crystals; crystals larger than expected for a given cooling time reflect slurries injection (Marsh, 2013).

The kinetics theory supposes that a new phase is nucleated by germ nuclei, which already exists in the old phase. The density of germinal nuclei decreases due to the conversion into growth nuclei of grains of the new phase, and their ingestion by growing grains. The relationship between the number of germinal nuclei, growth nuclei and transformed volume is expressed in terms of a characteristic timescale (Avrami, 1939).

The Johnson-Mehl-Avrami-Kolmogorov (JMAK) formalization, often referred to as the Avrami equation (Equation 1), as a simple sigmoidal function, was initially proposed to describe the phase evolution in synthetic material systems. However, many other transformations in the life, physical, and social sciences follow a similar pattern of nucleation and growth (Shirzad and Viney, 2023).

$$f(t) = 1 - e^{-kt^n} \qquad \text{Equation 1}$$

where *f(t)* is the fraction of material transformed as a function of time, and k and n are constants obtained from the model.

Scale times in magmatic processes vary from seconds to some years (*e.g.*, magma degassing) to hundreds or thousands of years (*e.g.*, magma residence time). Likewise, the timescale could increase from mafic to felsic magmas, which is proportional to the size of the system (Costa, 2021).

2. CSD Approach to nucleation-crystal growth processes in crystalline rocks

Crystal Size Distribution (CSD) is a stereology-based method that visualizes three-dimensional space via two-dimensional sections. The CSD, *i.e.*, the distribution of crystal size in three dimensions, is the number of crystals of a mineral per unit volume within a series of defined size intervals (Rannou and Caroff, 2010). Different practices are used in the analysis of the density and geometry of the crystal population, but crystals of interest are mainly separated and/or selected from orthogonal thin sections separated by a few microns (Bryon *et al.*, 1994, 1995) and with images obtained with X-Ray Micro-Tomography (XRmT; Jerram and Higgins, 2007).

CSD for batch systems is calculated using the Avrami equation (Equation 1) for crystallinity related to exponential variations in time of both

http://dx.doi.org/10.18268/BSGM2025v77n2a120325

nucleation and growth. Equation 1 describes the way solids transform from one phase to a different one at constant temperature, and the kinetics of crystallization if nucleation occurs randomly, concerning spatial coordinates (Avrami, 1939; Hort and Spohn, 1991; Marsh, 1998; Shirzad and Viney, 2023).

According to Babazadeh *et al.* (2021), the CSD pattern shape establishes a correlation between the rate of a constant magma supply that resembles batch melting systems, where melt volume decreases with time through perfect fractional crystallization. Slope, y-intercept, and maximum crystal-size in the CSD plots reflect the magmatic system maturity; from simple straight non-kinked CSDs in monogenetic systems to multiply kinked, piecewise continuous CSDs in well-established ones (Hersum and Marsh, 2007; Marsh, 1988).

The natural logarithm variation of the crystal population density (*i.e.*, the number of crystals per unit volume) with the crystal size yields a linear pattern under a consistent state of the open system (Figures 1a and 1b; Babazadeh *et al.*, 2021). CSD graph's slope relates the average growth rate of the crystal and the residence time through Equation 2 (Higgins, 2006; Marsh, 1988; Figure 1c).

$$m = -\frac{1}{G\tau} \qquad \text{Equation 2}$$

where m = slope; G = growth rate; and τ = residence time, then:

$$\tau = -\frac{1}{Gm} \qquad \text{Equation 3}$$

Residence time τ (Equation 3) is interpreted as the average time a crystal remains in the crystallization reservoir when it reaches its steady state before it is evicted. It considers that the number of extracted crystals and the mass of the incoming liquid are compensated (Castro-Dorado, 2015).

Physical processes changing in the magma chamber can influence the shape of the CSD. Crustal assimilation or the mixing of crystal populations during magma ascent from a deeper to a shallower reservoir, followed by residence and episodic coarsening in upper crustal storage levels, tends to inhibit crystal nucleation and growth, resulting in kinked or curved CSD patterns (Figures 1d and 1e; Babazadeh *et al.*, 2021).

CSD analysis has been applied in petrology from volcanic and metamorphic rocks, to lunar, Vesta and Mars rocks, and plutonic gabbroic bodies (Deb and Bhattacharyya, 2018; Díaz-Azpiroz and Fernández, 2003; Ennis and McSween, 2014; Filiberto *et al.*, 2018; Jerram *et al.*, 2009, 2010; Wang *et al.*, 2019; Yu *et al.*, 2023). CSD describes the behavior of olivine, amphiboles, pyroxenes, quartz, and potassium feldspars, but plagioclases are, by far, the most described minerals.

Crystal size has become the most prominent parameter analyzed in igneous texture studies of many different types of plutonic and volcanic rocks (Higgins, 2006). However, the felsic plutonic rocks case study is still scarce, standing out from the work in potassium feldspars at Cathedral Peak (Higgins, 2000). The complex texture of many granitoids is related to within-crystal heterogeneities, and the common alteration occurrence (Higgins, 2017).

In granitic rocks, plagioclase is usually the first phase crystallizing throughout the thermal history of the rock, varying from calcic to more sodic compositions (Bryon *et al.*, 1994). CSD analysis was obtained in plagioclase crystals for their abundance and distinctive geometric features (ratio of crystallographic axes). Further, in binary images, the outline of the plagioclases can be well distinguished from the mafic minerals. Also, plagioclases show stability in a wide range of pressure and temperature conditions, and micro-texture sensitivity to many physicochemical processes (Eskandari and Sadeghi, 2024). The other most common phases in granitoids, feldspar and quartz, however, have little contrast in X-ray absorption spectrum and cannot therefore be readily distinguished in 2D-3D images (Higgins, 2017).

http://dx.doi.org/10.18268/BSGM2025v77n2a120325

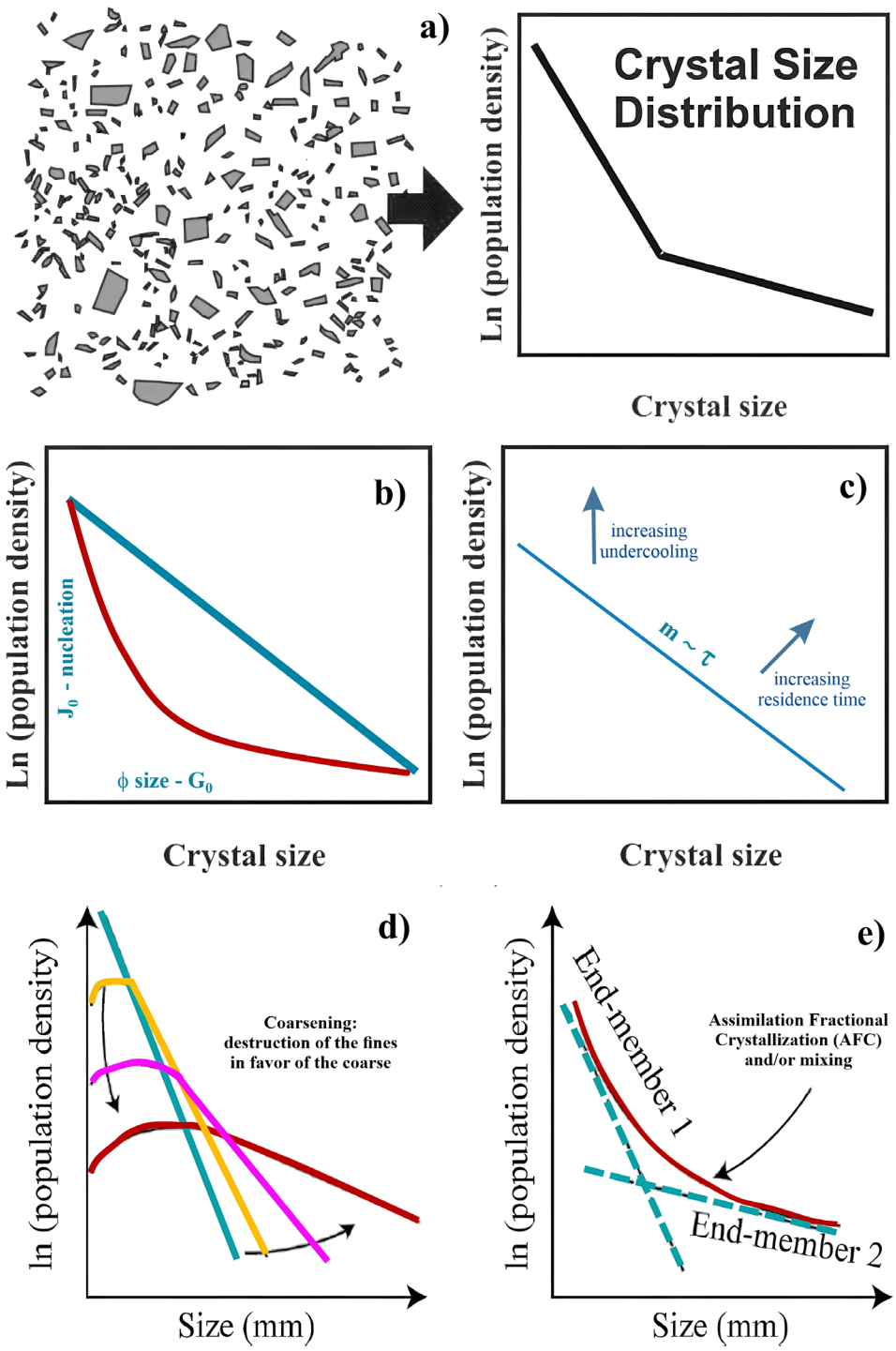

Figure 1 a) Crystal Size Distribution (CSD) is a quantitative determination of how many crystals of a certain size are found per unit volume [ρ]. b) Constant cooling rate (blue line): small sizes are more abundant than large ones [nucleation > growth]. In crustal magmatic systems, crystal growth dominates the nucleation rate (red line). c) The average residence time [τ] is interpreted as the time a crystal stands in the system before it is evicted. The higher cooling rate is related to the greater abundance of smaller crystals. Conversely, the longer crystal residence time regards, the lower the number of coarser crystals. d) The residence and growth of crystals at shallow levels of stagnation would tend to interrupt crystal nucleation and growth (blue line) and led to flexures and curvatures of the CSD patterns (marked with different colors). e) Crustal assimilation or mixing magma are related to crystal populations (blue lines) during the rise from a deep reservoir to a shallower one can result in concave up CSD patterns (red line). Modified from (Hersum and Marsh, 2007; Higgins, 2006; Jerram and Martin, 2008).

http://dx.doi.org/10.18268/BSGM2025v77n2a120325

In this work, we present CSD textural analysis methodology from eight different geochronological plutonic bodies from the cordilleran belt of southern Mexico. This CSD proxy was combined with geochemical and thermobarometric data to discuss the relationship between the crystallization processes and their emplacement conditions.

3. Plutonic assembly in southern Mexico: eight case studies of textural development in granitoid rocks

Belonging to the North American Cordillera, the western Mexico Mesozoic-Cenozoic geologic evidence shows arc magmatism episodes in diverse settings, such as crustal shortening and accretion, subduction erosion, tectonic extension, as well as switching from convergent to transform and divergent plate boundaries. Also, the existence of a long-lived magmatic arc, that vanished diachronically during Paleogene-early Miocene time, decreasing in age to the southeast, is preserved at the Sierra Madre del Sur (SMS; Morán-Zenteno *et al.*, 2018 and references herein).

The plutonic outcropped rocks are mainly composed of granitoid rocks *s.l.*, whose ages range from Jurassic to Miocene, emplaced into low-grade metamorphic and volcano-sedimentary rocks from Triassic-Cretaceous age of the Guerrero terrane (Morán-Zenteno *et al.*, 1999; Ortega-Gutiérrez *et al.*, 2014; Schaaf *et al.*, 1995; Centeno-García *et al.*, 2008; Figure 2)

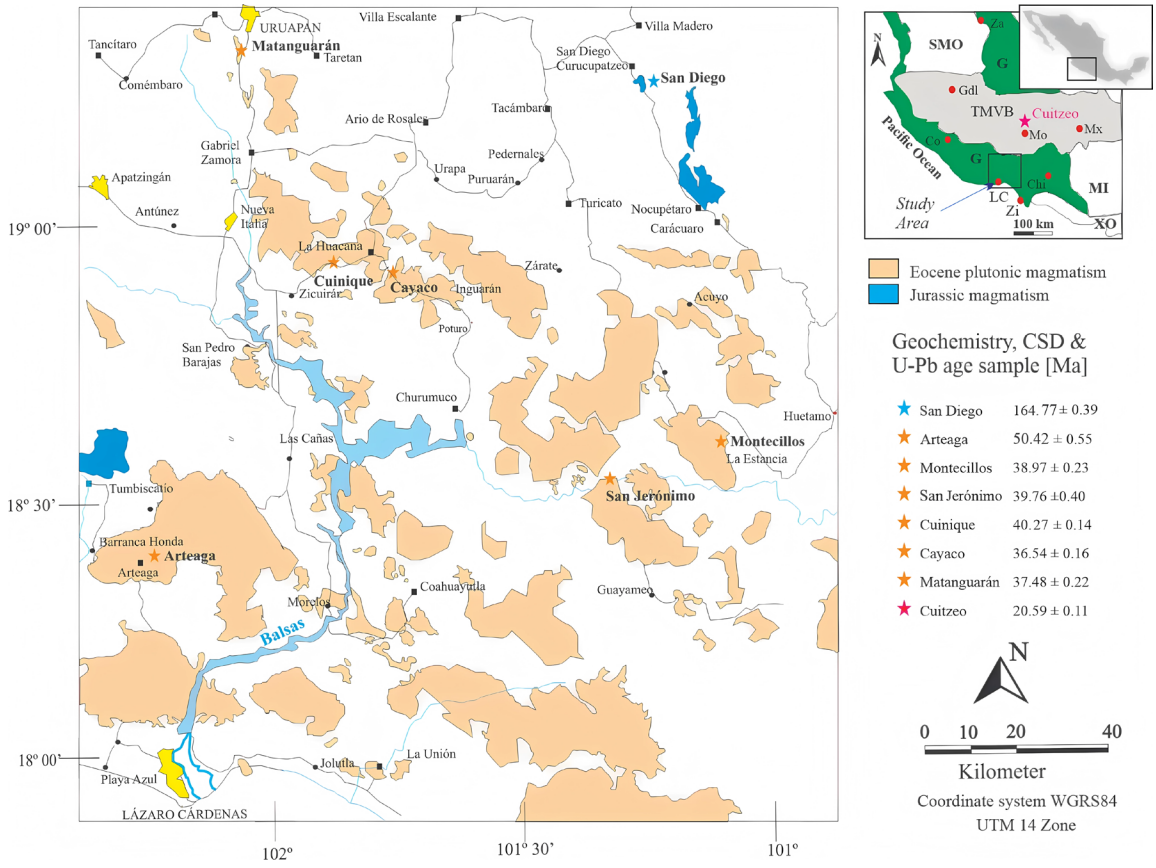

Figure 2 Location of studied plutons in southern México. For reference inset shows the Guerrero (G), Mixteco (MI), and Xolapa (XO) tectonostratigraphic terranes (Campa and Coney, 1983); Trans-Mexican Volcanic Belt (TMVB), Sierra Madre Occidental (SMO). Geographic references: Zacatecas (Za), Colima (Co), Guadalajara (Gdl), Morelia (Mo), Chilpancingo (Ch), Lázaro Cárdenas (LC) and Zihuatanejo (Zi) cities. Note the star for sampling points as well as the pink star point for the Cuitzeo Miocene intrusive location.

Two large groups of granitoid rocks outcrop along the Pacific margin in the Jalisco-Guerrero region as a part of the Zihuatanejo subterrane (Centeno-García *et al.*, 2008):

i) The Manzanillo-Jilotlán-Aquila Batholitic Complex (MJABC) is formed mainly by granite, granodiorite and tonalite felsic members, although also present are distinctive mafic members of gabbro, diorite, and quartz diorite compositions. Age of granitoids lies between 70 and 53 Ma, decreasing to the southeast, while also 115 and 84 Ma ages are reported in gabbroic rocks (Centeno-García *et al.*, 2008; Gómez-Rivera, 2019; Villanueva-Lascuráin *et al.*, 2016).

ii) The Lázaro Cárdenas-Zihuatanejo-Tecpan, the second group: La Mira, Arteaga, Montecillos and Zihuatanejo is constituted mainly by granitoid and pegmatitic rocks, with ages along the Eocene between 48 and 36 Ma (Schaaf *et al.*, 1995; Suazo-Cruz, 2020 and references therein).

This second group of Eocene granitoids is widespread towards the inland continent and is exposed sporadically associated even with its Eocene volcanic cover (Centeno-García *et al.*, 2008; Martini *et al.*, 2009). Montecillos, San Jerónimo, Guayameo, La Huacana and Matanguarán are Eocene granitoid localities that show good correlation and are exposed and dislocated by long tectonic extension structures. Matanguarán is the northernmost granitoid site and is located on the boundaries and overlain by volcanic sequences of the Transmexican volcanic belt (Corona-Chávez, 1999).

In another context, Jurassic plutons have also been reported in the San Diego Curucupatzeo and Tumbiscatío region (Guevara-Alday, 2020; Resendiz-Zarco, 2024), and as young as Miocene in the Cuitzeo region (Hernández-Bernal *et al.*, 2021), which, although belonging to diachronic magmatic arcs, all of them have calc-alkaline signatures. Based on compiled and new petrological, whole rock and chronological data (Figure 2 and Table 1) from samples of the San Diego Jurassic pluton, Arteaga, Montecillos, San Jerónimo, La Huacana and Matanguarán Eocene intrusives and Cuitzeo Miocene xenolith, we carried out calculations and CSD patterns to integrate a framework for emplacement constraints.

4. Methods

4.1. MAJOR AND TRACE GEOCHEMISTRY AND ZIRCON ISOTOPIC DATING

Around 200 g of fresh pulverized sample material of each granitic sample were used for geochemical analyses. Major elements were determined at the Laboratorio Nacional de Geoquímica y Mineralogía (LANGEM at Universidad Nacional Autónoma de México -UNAM) by X-ray fluorescence spectroscopy (XRF) using a Siemens SRS-3000 instrument. Trace element abundances were acquired using a Thermo Series XII instrument of the Laboratorio de Estudios Isotópicos (LEI), by inductively coupled plasma mass spectrometry (ICP-MS) at the Instituto de Geociencias (IGC-UNAM). The zircon crystals obtained from a granulated portion were analyzed employing a Resonetics M050 excimer laser coupled with a Thermo Xseries quadrupole ICP-MS, at the laser ablation system of the Laboratorio de Estudios Isotópicos (LEI-IGC-UNAM).

4.2. PRESSURE AND TEMPERATURE CONDITIONS

Quantitative electron-microprobe analyses were done in wavelength-dispersion mode with a JEOL JXA-8200 electron microprobe, at the Department of Earth Sciences of the University of Milan (ESD-MI).

Pressure calculation was carried out using the Al-in-hornblende barometry formulation (Mutch *et al.*, 2016) using amphibole measurements.

The temperature calculation was performed from pressure-dependent expressions in plagioclase- amphibole pairs (Anderson *et al.*, 2008). Ti-in zircon temperature was calculated with the Ferry and Watson (2007) equation.

http://dx.doi.org/10.18268/BSGM2025v77n2a120325

Table 1. Location, name and age of the plutonic bodies studied.

Name	Location	Rock type	Age [Ma]	Method	Age reference	Distance to the trench [km]*
San Diego	19.26883 -101.12524	Granodiorite	164.77 ± 0.39	U-Pb	This work	185
Arteaga	18.38886 -102.22464	Diorite-Granodiorite	50.42 ± 0.55	U-Pb	This work	45
Montecillos	18.63649 -101.09865	Granodiorite	38.97 ± 0.23	U-Pb	This work	125
San Jerónimo	18.5283 -101.4683	Granodiorite	39.76 ±0.4	U-Pb	(Martini *et al.*, 2009)	85
La Huacana 1 Cuinique	18.93117 -101.87909	Monzonite-Quartmozonite	40.27 ± 0.14	U-Pb	This work	125
La Huacana 2 Cayaco	18.90669 -101.76558	Diorite	36.54 ± 0.16	U-Pb	This work	125
Matanguarán	19.33546 -102.07931	Granodiorite	37.48 ± 0.22	U-Pb	This work	160
Cuitzeo	19.8762 -101.2343	Granite	20.59 ± 0.11	U-Pb	(Hernández-Bernal *et al.*, 2021)	250

4.3. CRYSTAL SIZE DISTRIBUTION PLOTS

Cylinders one inch tall by one inch in diameter of the chosen plutonic bodies' samples were used. They were analyzed by x-rays tomography technique in LUMIR (University Lab of X-Rays Micro-tomography at Geosciences Institute, UNAM), based on the attenuation of beams that penetrate the sample (Jerram and Higgins, 2007).

The geometry of the crystal population was obtained from a set of X-ray tomography images of the samples using ImageJ public domain software. From bidimensional data (2D) returned by the ImageJ software, the number of crystals per mm^3 as a function of size was valued using the stereological procedure of *CSD Corrections 1.61 ver.* software (available at http://www.uqac.ca/mhiggins/csdcorrections.html).

The input parameters include a massive fabric and the average 3-D aspect ratio (AR) of the plagioclase crystals 1:2:5 (S, I, L), values in the range of those reported by (Babazadeh *et al.*, 2021; Garrido *et al.*, 2001; Holness *et al.*, 2020) for phaneritic rocks.

5. Results

5.1. MAJOR AND TRACE GEOCHEMISTRY AND ZIRCON ISOTOPIC DATING

The abundance of rock-forming minerals and major element diagrams indicate diorite, monzonite, granodiorite and granite composition (Figure 3a and Table 1).

All of them show a calc-alkaline signature. The Shand's Index of the Cenozoic plutons is metaluminous, whereas the Jurassic body is clearly peraluminous (Figure 3b). The chondrite normalized REE plot in Figure 3c shows a typical signature of magmatic arc, LREE enriched relative to flat HREE with a negative Eu anomaly suggesting a previous removal of plagioclases in parental magma.

The isotopic U-Pb dating on zircon crystals gives new ages for six plutons. The result ranges from 164.7 to 20.6 Ma.

The new calculated ages are shown in Figure 4. Note the almost complete absence of inherited zircons.

http://dx.doi.org/10.18268/BSGM2025v77n2a120325

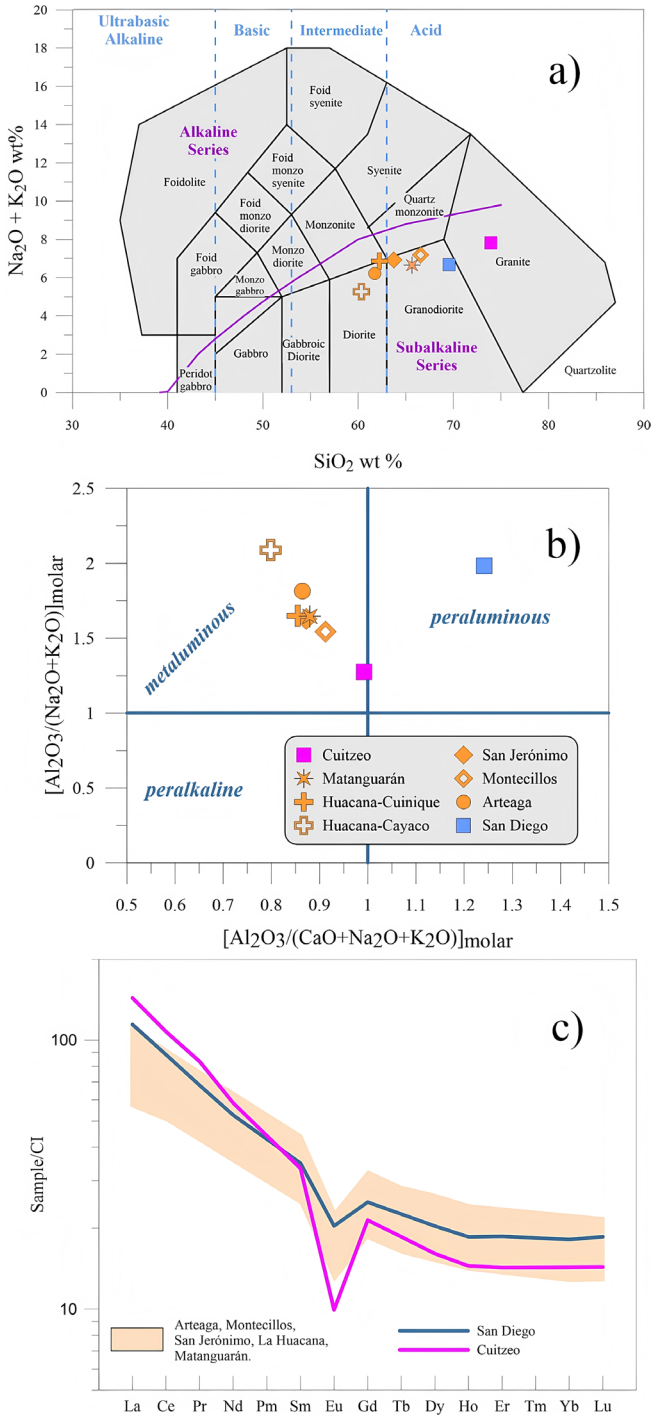

Figure 3 a) Geochemical TAS diagram showing the subalkaline type and classification. b) Most plutons are metaluminous, except for the Jurassic San Diego pluton with a peraluminous signature. c) REE pattern display LREE enrichment over a flat HREE and distinctive Eu anomaly typical of the magmatic arc setting.

5.2. PRESSURE AND TEMPERATURE CONDITIONS

The calculated pressure and temperature obtained from Mg-hornblende amphiboles and plagioclases pairs range from 1.0 to 2.8 kbar and 684 to 818 °C, indicating shallow intrusion conditions (Figure 5a and Table 2). Also, the saturation temperature recorded in zircons was obtained, always being higher than those obtained with amph-plg pairs (Figure 5b and Table 2). Zircon saturation thermometry, between 693 and 921 °C, provides a means of estimating magma temperatures. The > 800 °C zircon temperatures are considered "hot" inheritance-poor granitoids (Miller *et al.*, 2003), in agreement with the Weighted Mean age plots (Figure 4) that indicate almost absence of inherited zircon crystals.

5.3. CRYSTAL SIZE DISTRIBUTION PLOTS

Data related to the natural logarithm of crystal population density were plotted versus crystal length (Figure 6 and Table 3). The CSD plots for different pluton samples exhibit curved patterns. The crystal population $\log_{density}$ of described granitic rocks ranges from +8 to -5.

We constrain the curved CSD patterns to be represented by two linear segments as other authors do (Bell *et al.*, 2023; Hamzah *et al.*, 2018; Marsh, 1998); one segment chosen for small crystals < 0.5 mm, and another segment for large crystals size > 0.5 mm. Thereafter, we used both segments to calculate the approximate storage times necessary to accomplish the observed crystal growth.

From these two segments and linear regression adjusted, it can be observed that crystals with higher nucleation rates produce fine grain size and steeper CSD slopes. Coarser grain size, on the other hand, reflects low nucleation density and implies a gentler CSD slope (Figure 6).

Table 3 contains the path, slope, and intercept values calculated with Grapher® software. The residence time τ calculated with Equation 3 considers growth rate G equal to 10^{-10} mms^{-1} (Marsh, 1988). The calculated average residence time from CSD slopes of plagioclase crystals is 17

http://dx.doi.org/10.18268/BSGM2025v77n2a120325

Table 2. Major and REE contents for granitic plutons, zircon-Ti temperature (Ferry and Watson, 2007), and hornblende-plagioclase thermobarometry (Anderson *et al.*, 2008; Mutch *et al.*, 2016). 1: This work; 2: Hernández-Bernal *et al.* (2021).

Pluton	San Diego	Arteaga	Montecillos	San Jerónimo	Cuinique	Cayaco	Matanguarán	Cuitzeo
sample	GSD-8-10	GATG-01	GMTC-01	GSJ-01	GHUA-01	GHUA-02	GMTG-01	G-CUITZ-01
Reference	1	1	1	1	1	1	1	2
oxide wt %								
SiO_2	68.40	61.53	66.21	63.26	61.35	59.80	65.16	73.71
TiO_2	0.59	1.07	0.66	0.86	1.06	0.83	0.68	0.27
Al_2O_3	15.92	15.95	14.78	15.18	14.90	15.06	14.69	13.62
Fe_2O_3t	3.87	6.99	5.11	6.24	7.21	7.46	5.52	2.06
MnO	0.05	0.10	0.07	0.09	0.10	0.11	0.07	0.02
MgO	1.49	2.24	1.72	2.11	2.32	4.06	2.15	0.51
CaO	2.64	5.31	3.64	4.45	4.62	6.41	4.27	1.67
Na_2O	3.54	3.70	3.27	3.36	3.04	2.78	3.18	4.00
K_2O	2.03	2.50	3.88	3.51	3.73	2.44	3.42	3.81
P_2O_5	0.06	0.29	0.13	0.19	0.25	0.14	0.11	0.05
PXC	1.42	0.33	0.52	0.74	1.31	0.80	0.75	0.17
Total	100.00	100.00	100.00	100.00	99.89	99.90	100.00	99.88
REE [µg/g]								
La	27.1	20.2	19.9	26.5	24.3	13.5	20.2	34.0
Ce	54.1	44.7	41.9	55.3	53.0	31.1	42.1	65.8
Pr	6.5	6.0	5.3	7.2	7.1	4.1	5.4	7.9
Nd	24.6	24.9	21.1	28.6	28.7	16.5	21.0	27.3
Sm	5.3	5.7	4.8	6.4	6.7	3.8	4.7	5.1
Eu	1.2	1.3	0.9	1.1	1.1	0.7	0.9	0.6
Gd	5.1	5.5	4.7	6.0	6.6	3.8	4.6	4.4
Tb	0.8	0.9	0.8	1.0	1.1	0.6	0.8	0.7
Dy	5.2	5.2	4.7	5.8	6.7	3.9	4.6	4.1
Ho	1.1	1.0	0.9	1.2	1.4	0.8	0.9	0.8
Er	3.1	2.9	2.7	3.3	3.9	2.2	2.7	2.4
Yb	3.1	2.9	2.8	3.3	3.8	2.2	2.7	2.4
Lu	0.5	0.4	0.4	0.5	0.6	0.3	0.4	0.4
T °C [Zr Ti] (aSi = 1, aTi = 0.6)								
n	32	26	29	n.r.	34	34	31	29
Ti [ppm]	10.6	12.4	17.3	n.r.	12.6	15.1	29.3	3.0
T [°C]	803	819	856	n.r.	820	840	921	693
Pressure [kbar] and T [°C]								
P [kbar]	n.r.	2.8	2.1	n.r.	1.8	1.2	1.0	1.1
T [°C]	n.r.	794	818	n.r.	798	708	684	643

to 67 years for small sizes, < 0.5 mm, and 86 to 187 years for > 0.5 mm (Table 3).

6. Discussions and conclusions

6.1. CRYSTAL SIZE DISTRIBUTION PLOTS AND MIXING PROCESSES

As mentioned earlier, a linear slope on a CSD diagram indicates simple cooling of magma, but if the diagram exhibits hump-shaped, kinks or changes of slope, added processes must have been placed over upon the cooling, such as mixing of magmas or coarsening of individual mineral grains (Higgins, 2006). CSD diagrams of the described plutons (Figure 6 and Table 3) do not display straight lines. The upward concave lines suggest the magma mixing in a magma chamber prior to or during ascent and emplacement (see Figure 1e). The flexure or narrow humps on smaller crystal sizes in Arteaga and San Jerónimo CSD curves agree with the presence of Mafic Microgranular Enclaves (MMEs) in macro and microscopic scales, respectively (Figures 7b and 8c).

http://dx.doi.org/10.18268/BSGM2025v77n2a120325

The presence of the MMEs probably is related to a hotter mafic magma that cools rapidly when it meets colder felsic host magma, producing a short-lived large nucleation stage (humped curve). In none of the described cases, straight or nearly straight CSD curves suggest that thermal equilibrium was achieved during the interaction of mafic and felsic magma. Instead, the measurements produced curved CSD lines (Figures 6, 7 and 8 and Table 3), pointing to magma mixing/mingling as a ubiquitous process.

6.2. CRYSTAL SIZE DISTRIBUTION PLOTS AND RESIDENCE TIME

In this study, the calculated residence time in plagioclase crystals, from 85 to 187 years, particularly those for crystals > 0.5 mm, agree with values of residence time obtained in plutonic mafic and felsic bodies, phenocrysts, and central areas of dikes tens of meters thick that ranges from 117 to 375 years (Ashok *et al.*, 2022; Babazadeh *et al.*, 2019, 2021; Deb and Bhattacharyya, 2018; Ngonge *et al.*, 2013; Nugroho *et al.*, 2019). Furthermore, the residence times obtained in this work, of the order of 10^2, are comparable to the duration of diffusion and the mixing and assimilation times of magma for intermediate to silicic systems, of the order of 10^1-10^2 (Cooper, 2019; Costa, 2021).

According to Figure 1c, the higher slope of the smaller plagioclase population compared to the larger size population suggests that the smaller ones underwent higher undercooling in shallower crustal regions and shorter residence times.

6.3. RESIDENCE TIME VERSUS P-T

It seems that there is no direct relationship between barometric values versus residence times. The calculated residence time of the larger plagioclase crystals (> 0.5 mm), from 85 to 187 years, may reflect a stationary crystallization depth of plagioclases (see Cashman, 2020).

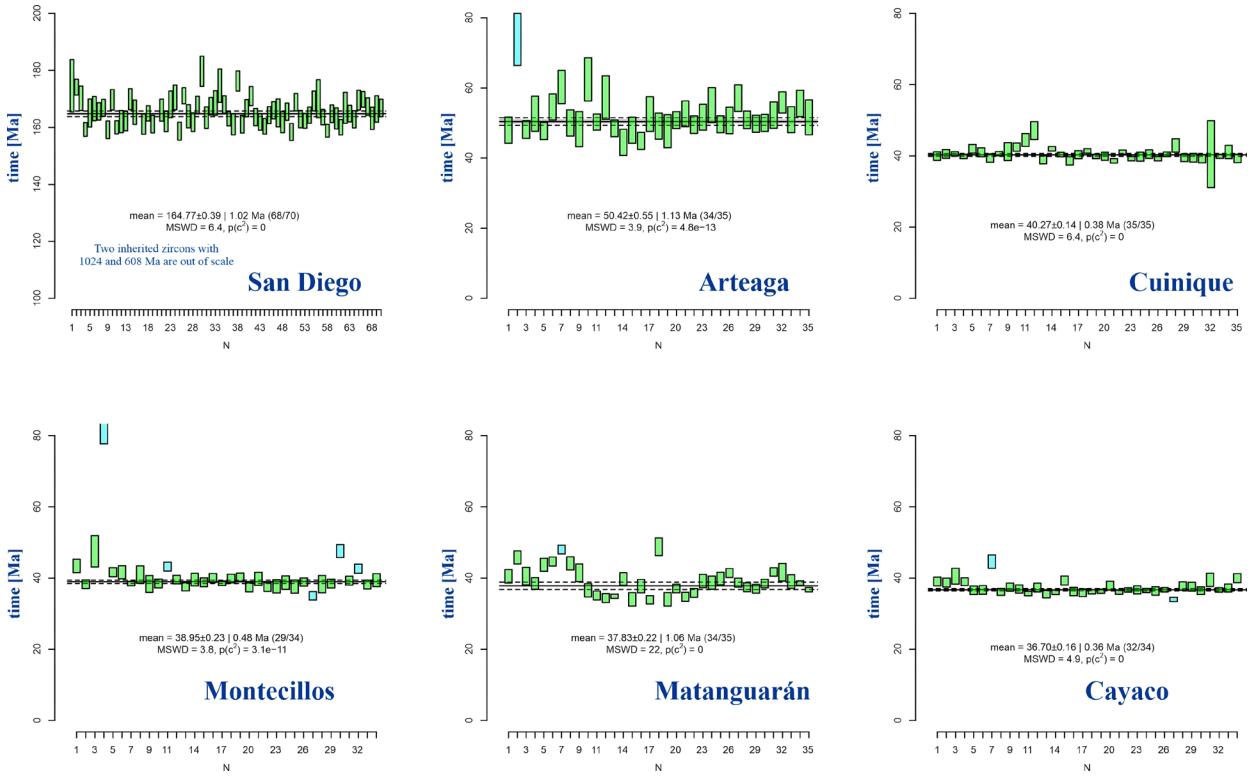

Figure 4 Mean Weighted ages obtained in zircon crystals.

http://dx.doi.org/10.18268/BSGM2025v77n2a120325

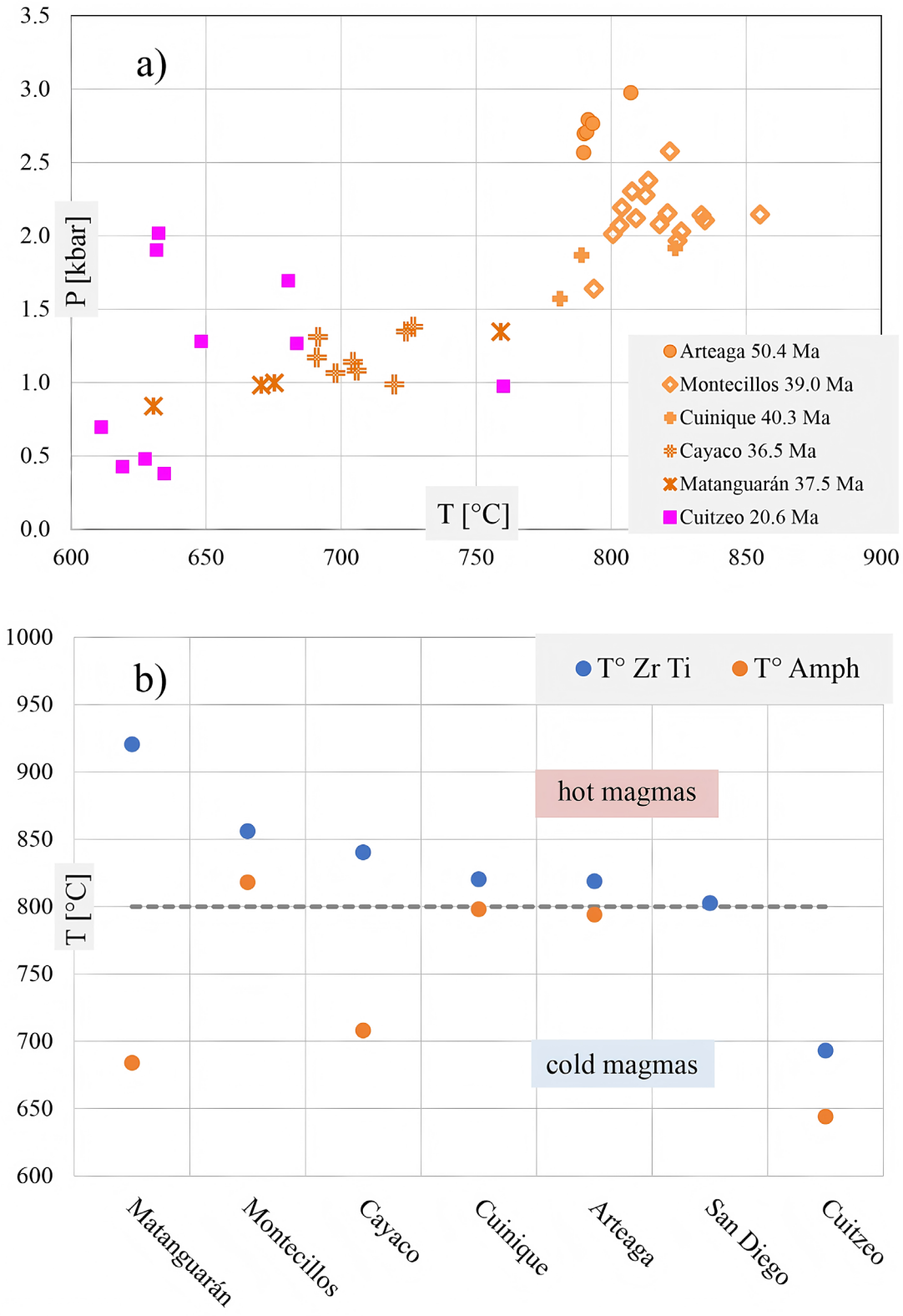

Figure 5 a) P-T diagram of selected amph-plg pairs. Cuitzeo is marked in pink to distinguish it as a younger body (20 Ma) and due to its greater distance from the trench (250 km). b) Two thermometers, Zr and amph-plg, compared showing "hot" and "cold" regions of magmas (Miller *et al.*, 2003).

http://dx.doi.org/10.18268/BSGM2025v77n2a120325

Table 3. Crystal size distribution (CSD) parameters of plagioclases for granitic plutons. R2 = Coefficient of determination; Intercept = proportional to nucleation density; τ = Residence time. When the letters G or E are indicated, it refers to samples analyzed considering only the granitoid rock G, the enclave E or both phases G+E.

Pluton	Sample	R^2	Intercept	slope	τ [years]	R^2	Intercept	slope	τ [years]
		0.1-0.5 mm				0.5-2.5 mm			
San Diego	GSD	1.00	6.39	-17.4	18.2	0.99	2.33	-2.999	105.7
Arteaga	GATG-G	0.96	5.09	-9.837	32.2	0.99	1.96	-3.162	100.3
	GATG-E	0.93	4.86	-6.517	48.7	1.00	2.22	-3.141	101.0
	GATG E+G	1.00	6.19	-9.316	34.0	0.97	2.99	-3.315	95.7
Montecillos	GMTC	0.96	6.80	-12.31	25.8	0.98	2.06	-2.619	121.1
San Jerónimo	GSJ G+ E	0.84	4.55	-4.741	66.9	0.99	3.26	-3.643	87.0
	GSJ G	0.96	7.49	-17.47	18.2	0.99	3.75	-3.699	85.7
Cuinique	GH1	0.97	8.41	-15.74	20.1	0.95	1.59	-2.065	153.6
Cayaco	GH2	0.97	3.96	-9.974	31.8	0.98	-0.37	-1.694	187.2
Matanguarán	GMTG	0.97	7.66	-18.8	16.9	0.96	3.07	-3.175	99.9
Cuitzeo	GXCZ	0.95	4.80	-11.46	27.7	1.00	2.21	-3.283	96.6

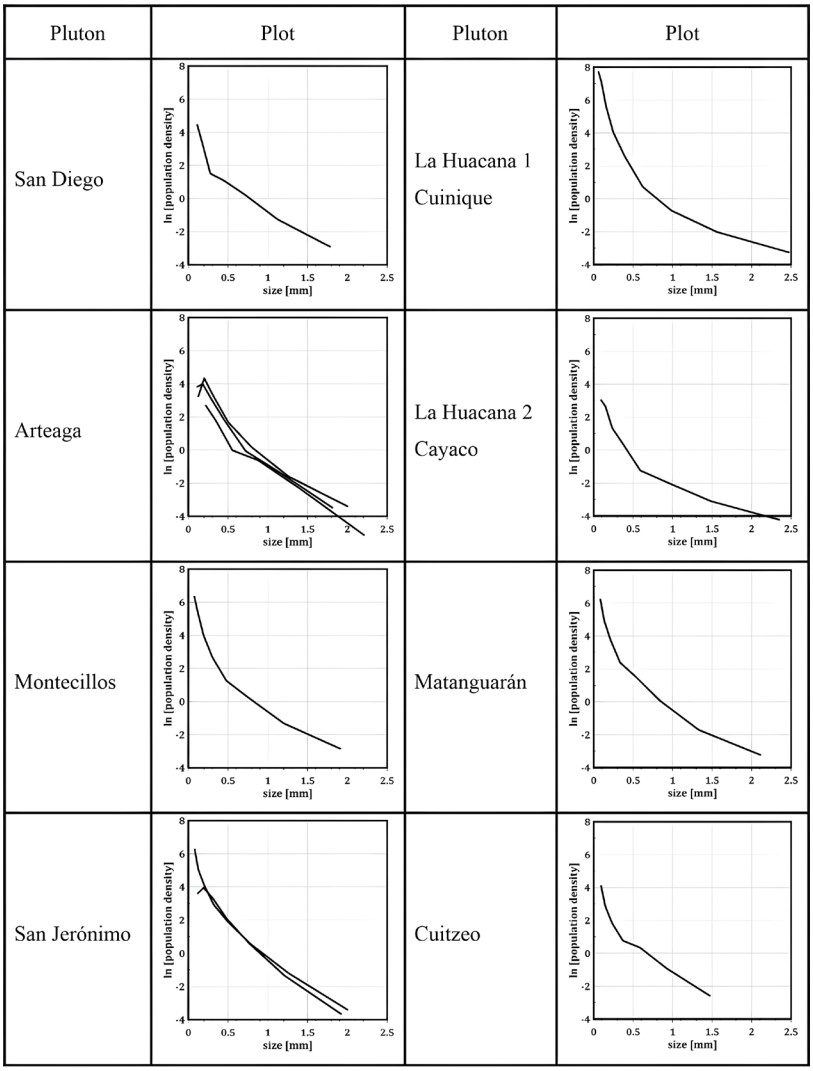

Figure 6 Natural logarithm of crystal population density versus crystal length (mm). For comparison, all plots have same scales.

http://dx.doi.org/10.18268/BSGM2025v77n2a120325

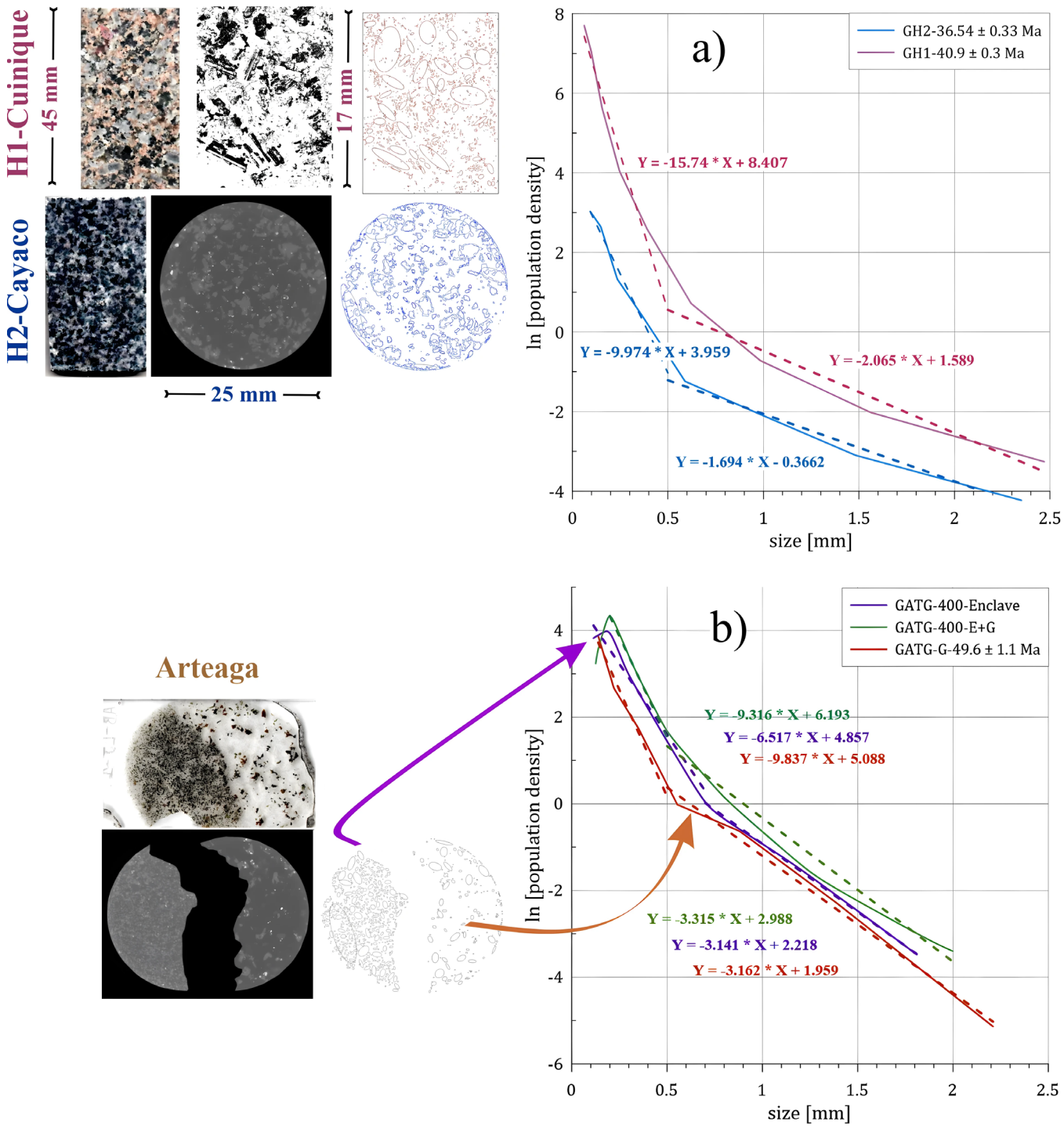

Figure 7 Crystal size distribution of plagioclase, thin slides and XRmT images as well as the ellipses calculated for plagioclase crystals whose geometry is reflected in CSD diagrams. a) Cuinique and Cayaco plutons in La Huacana region. The H1 CSD analysis was performed using a thin slide image. b) Note the macroscopic mafic microgranular enclaves for Arteaga pluton and its characteristic humped form at the finest sizes.

http://dx.doi.org/10.18268/BSGM2025v77n2a120325

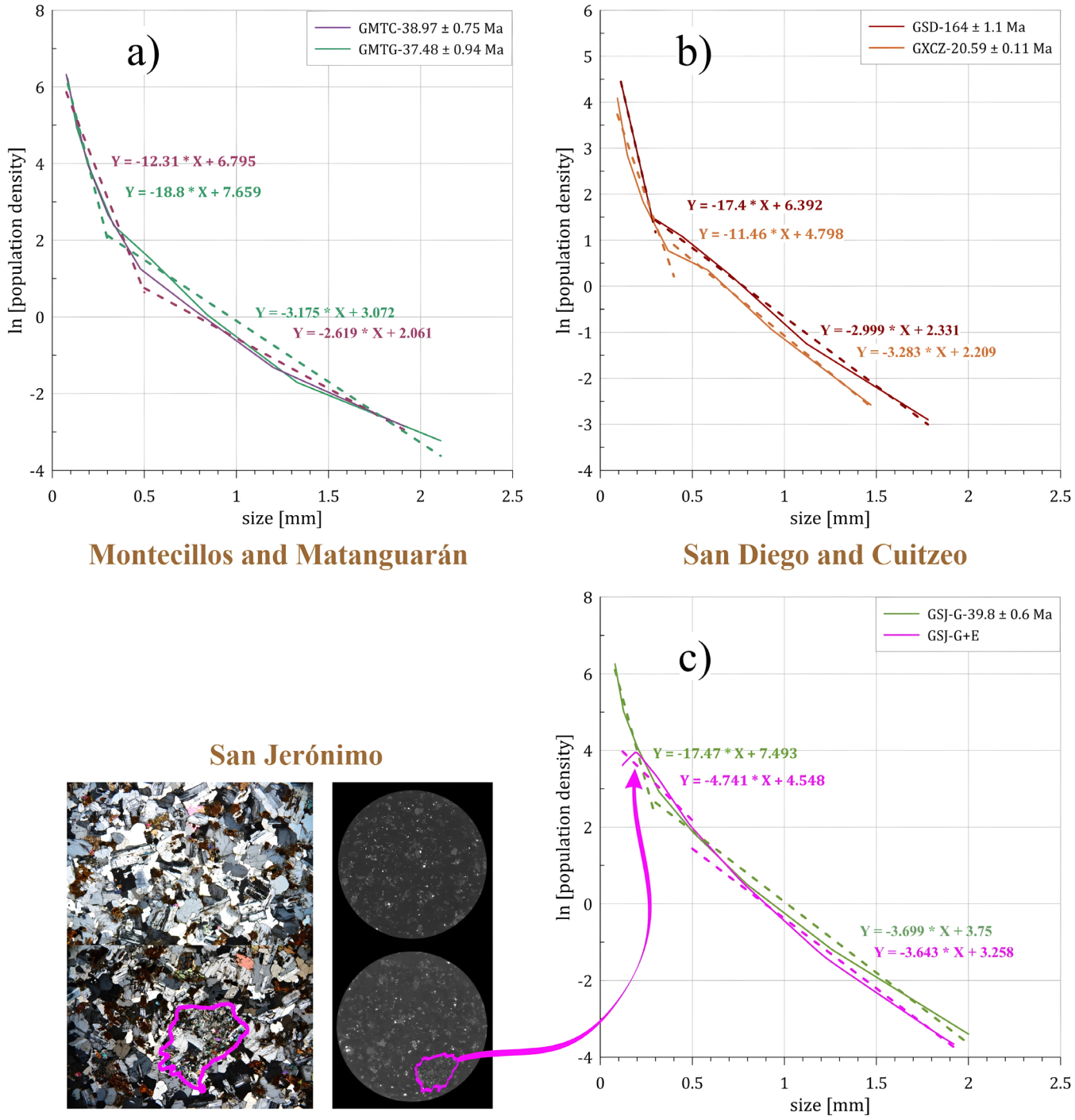

Figure 8 Crystal size distribution of plagioclase, thin slides and XRmT images as well as the ellipses calculated for plagioclase crystals whose geometry is reflected in CSD diagrams. a) Montecillos and Matanguarán samples; b) San Diego and Cuitzeo samples. In c) note the microscopic MMEs for San Jerónimo pluton and its characteristic humped form at the finest sizes. The MMEs are not visible in the hand sample.

http://dx.doi.org/10.18268/BSGM2025v77n2a120325

Figure 9a shows the behavior of residence time τ versus temperature, calculated with the amph-plg pair or with the saturation Zr system. Two trends are observed; the first corresponds to the Matanguarán, Montecillos, Arteaga and Cuitzeo plutons, which, in both thermometers, suggests that the bodies with lower temperatures stagnate for longer times and vice versa, the crystals of the magmas with higher temperatures will be removed in less time. The similarity of the values of the amphibole and zircon thermometers in the Cuitzeo, Arteaga and Montecillos plutons and the empirical relationship with the residence time suggest that the cooling trajectory did not experience great thermal contrasts, despite the possible mixing of magmas.

Although the Matanguarán body is related to this trend of higher temperature versus shorter residence time, it is worth to note a relative discrepancy between the temperature values obtained by Ti-in zircon (Ferry and Watson, 2007) and plagioclase-hornblende thermometer (Anderson *et al.*, 2008). In addition, this sample presents a textural complexity that apparently suggests mixing magma and latest hydrothermal alteration, which makes difficult a simple CSD interpretation.

On the other hand, the second complex trend corresponds to the data of both thermometers obtained in the Cayaco and Cuinique bodies in the La Huacana area. They also follow this inverse trend between residence time and temperature, but with a shift towards longer residence times. This suggests that both plutons emplaced shallowly as a "hot" magma and that the cooling pattern of the older Cuinique body (40 Ma) was modified by the intrusion of the younger Cayaco body (36 Ma) at the same cortical level (1.8-1.2 kbar).

Figure 9b suggests that the residence time is also inversely proportional to the silica content, but all the values obtained lie in the same time order, 10^1 to 10^2, so it is difficult to compare with the temporality of processes reported by Costa (2021).

6.4. MAGMA PROCESSES IN SW MÉXICO

The studied plutons are representative of diachronic magmatic arc suites, from Jurassic to Neogene periods, based on their mineralogical content, magmatic series classification and REE paths. The magmatic arc tectonic setting has been imposed in the western region of México since Mesozoic times to the present. The P-T conditions indicate a surface emplacement < 3 kbar. Additionally, the isotopic values of $^{87}Sr/^{86}Sr_i$ of Cretaceous and Paleogene plutons of the Sierra Madre del Sur are variable, but most lie between = 0.704 and 0.705, and the epsilon Nd_i generally has positive values (Morán-Zenteno *et al.*, 2018). The isotopic values of the Miocene Cuitzeo body also lie within these ranges (Hernández-Bernal *et al.*, 2021). Therefore, although in this work we do not discuss isotopic data, we consider that the emplacement occurred in a young crust for a long time and that given its predominantly felsic character, both the low density and low temperature contrasts favored the magmas to stagnate for periods of tens or hundreds of years. The plots of CSD for these granitoids show open systems behaviors with no constant conditions and no simple cooling stage.

These residence times are the first calculated for plutonic bodies in Mexico. The data obtained agree with those reported by other authors for igneous bodies, from 117 to 375 years, as mentioned above. According to the data analyzed in this work, the age of the rocks, the distance to the actual trench, and the depth have no imprint on the geometry of the CSD. No trace of pressure effect is evident in the residence times of the selected intrusive bodies, which record a very narrow pressure range. However, the temperature recorded by two different thermometers shows greater contrast, and thus, an inverse relationship is observed between the crystal stagnation time and the magma temperature. The likeness in the described bodies of the crystal growth times of plagioclases, mixing processes, plus shallow emplacement conditions indicate that the

http://dx.doi.org/10.18268/BSGM2025v77n2a120325

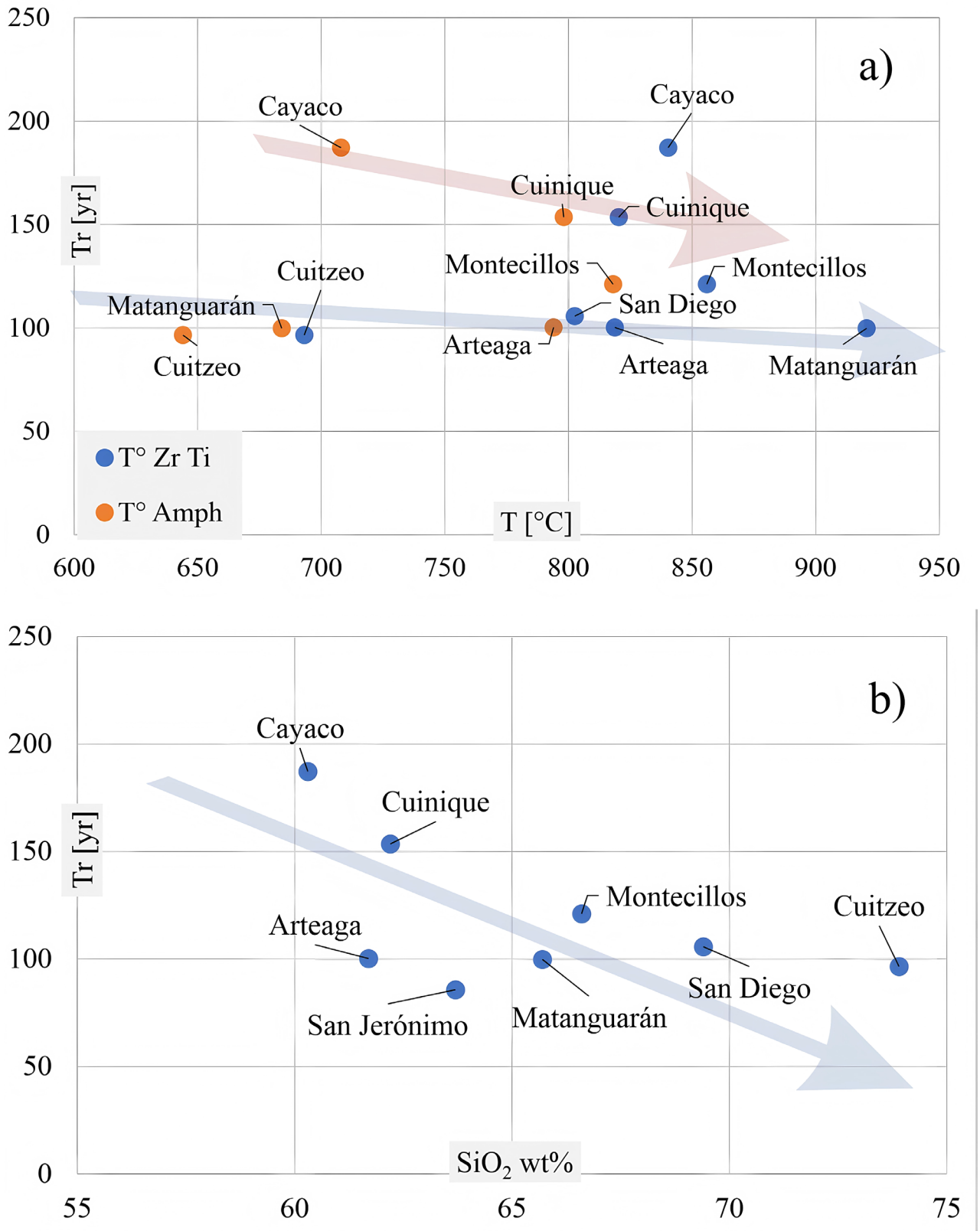

Figure 9 Residence time (Tr/yr vs. temperature (T °C) and SiO_2 (wt%). a) A subtle inverse relationship between residence time calculated versus temperature of plutons is noted. b) A raw inverse relationship between silica temperature and time is also noted.

http://dx.doi.org/10.18268/BSGM2025v77n2a120325

dynamics of the magmatic processes that occurred since the Jurassic in the southern margin of México are compatible with diachronous magmatic arcs, although the difference in crustal thickness and the direction and rates of magmatic migration are still issues that need to be investigated with other tools.

We argue that any pluton body requires to be analyzed in detail. Specially a careful 3D geometric and volumetric description of different generations of amphiboles-plagioclases assemblages is required, which may insight on different stages of crustal stagnation and ascent in the La Huacana (Cuinique and Cayaco) and Matanguarán regions, which present complex characteristics. It is convenient to determine whether other minerals, such as amphiboles or K-feldspars, retain the signature of mixture or magma mingling.

Future careful study of three-dimensional (3D) information of the textures during the solidification of these bodies will allow quantifying their role in the compositional differentiation of silicic magmas.

Contributions of authors

MH and PC contributed to conceptualization, the fieldwork and writing—original draft preparation. GS, ER and LR contributed to the methodology and carried out the fieldwork. SP contributed by obtaining and discussing accurate thermobarometric data.

Financing

MS and PC thank project PAPIIT-IN114521 for financial support.

Acknowledgements

The authors are also thankful to Lozano-SantaCruz and Ofelia Pérez-Arvizu for analytical support in XRF and ICPMS analyses, respectively. Isotopic measurements of U-Pb, were carried out by Carlos Ortega- Obregón. The XRmT runs were performed by Dante Arteaga-Martínez and the extraction of zircon crystals was supervised by Consuelo Macías-Romo. Comments from two reviewers helped to substantially improve the content of this paper.

Conflicts of interest

The authors declared that they have no competing interests.

Handling editor

Avto Gogichaishvili.

References

Anderson, J.L., Barth, A.P., Wooden, J.L., Mazdab, F., 2008, Thermometers and thermobarometers in granitic systems: Reviews in Mineralogy and Geochemistry, 69, 121–142. https://doi.org/10.2138/rmg.2008.69.4

Ashok, Ch., Santhosh, G.H.N.V., Ratnakar, J., Dash, S., 2022, Magma Mixing and Mingling during Pluton Formation: A Case Study through Field, Petrography and Crystal Size Distribution (CSD) Studies on Sirsilla Granite Pluton, India: Journal of the Geological Society of India, 98(6), 815–821. https://doi.org/10.1007/s12594-022-2072-4

Aspillaga, L., Jan-Bautista, D., Daluz, S.N., Hernandez, K., Renta, J.A., Lopez, E.C.R., 2023, Nucleation and Crystal Growth: Recent Advances and Future Trends: Engineering Proceedings, 56(1). https://doi.org/10.3390/ASEC2023-15281

Avrami, M., 1939, Kinetics of phase change. I: General theory: The Journal of Chemical Physics, 7(12), 1103–1112. https://doi.org/10.1063/1.1750380

Babazadeh, S., Furman, T., Cottle, J.M., Raeisi, D., Lima, I., 2019, Magma chamber evolution of the Ardestan pluton, Central Iran: evidence

from mineral chemistry, zircon composition and crystal size distribution: Mineralogical Magazine, 83(6), 763–780. https://doi.org/10.1180/mgm.2019.44

Babazadeh, S., Ghalamghash, J., Furman, T., D'Antonio, M., Raeisi, D., 2021, The Oligocene Avaj volcanic – plutonic complex of Central Iran: A record of magma evolution and mineral equilibria: Journal of Asian Earth Sciences, 222, 104962. https://doi.org/10.1016/j.jseaes.2021.104962

Bell, S.K., Joy, K.H., Pernet-Fisher, J.F., Hartley, M.E., 2023, Investigating the crystallization history of Apollo 15 mare basalts using quantitative textural analysis: Meteoritics and Planetary Science, 58(7), 955–977. https://doi.org/10.1111/MAPS.14032

Bryon, D.N., Atherton, M.P., Hunter, R.H., Parsons, I., 1994, The description of the primary textures of "Cordilleran" granitic rocks: Contributions to Mineralogy and Petrology, 117(1), 66–75. https://doi.org/10.1007/BF00307730

Bryon, D.N., Atherton, M.P., Hunter, R.H., 1995, The interpretation of granitic textures from serial thin sectioning, image analysis and three-dimensional reconstruction: Mineralogical Magazine, 59(395), 203–211. https://doi.org/10.1180/minmag.1995.059.395.05

Campa, M.F., Coney, P.J., 1983, Tectono-stratigraphic terranes and mineral resource distributions in Mexico: Canadian Journal of Earth Sciences, 20(6), 1040–1051. https://doi.org/10.1139/E83-094

Cashman, K.V., 2020, Crystal Size Distribution analysis of volcanic samples: advances and challenges: Frontiers in Earth Science, 8, 291. https://doi.org/10.3389/feart.2020.00291

Castro-Dorado, A., 2015, Petrografía de rocas ígneas y metamórficas: México, Paraninfo, 276 p.

Centeno-García, E., Guerrero-Suastegui, M., Talavera-Mendoza, O., 2008, The Guerrero Composite Terrane of western Mexico: Collision and subsequent rifting in a supra-subduction zone, in Draut, A.E., Clift, P.D., Scholl, D. (eds.), Formation and Applications of the Sedimentary Record in Arc Collision Zones:U.S.A., The Geological Society of America, 279–308. https://doi.org/10.1130/2008.2436(13)

Cooper, K.M., 2019, Time scales and temperatures of crystal storage in magma reservoirs: implications for magma reservoir dynamics: Philosophical Transactions. Series A, Mathematical, Physical, and Engineering Sciences, 377(2139). https://doi.org/10.1098/RSTA.2018.0009

Corona-Chávez, P., 1999, El basamento litológico y tectónico del estado de Michoacán, in Garduño-Monroy, V.H., Corona-Chávez P. Israde-Alcántara, I., Menella, L., I., Chiesa, S., Bigioggero, B. (eds.), La carta geológica del estado de Michoacán, escala 1: 250 000 en 4 hojas con notas explicativas: México, Universidad Michoacana de San Nicolás de Hidalgo, 1–45.

Costa, F., 2021, Clocks in magmatic rocks: Annual Review of Earth and Planetary Sciences, 49, 231–252. https://doi.org/10.1146/annurev-earth-080320-060708

Deb, T., Bhattacharyya, T., 2018, Interaction between felsic granitoids and mafic dykes in Bundelkhand Craton: A field, petrographic and crystal size distribution study: Journal of Earth System Science, 127(7), 1–14. https://doi.org/10.1007/s12040-018-1003-7

Díaz-Azpiroz, M., Fernández, C., 2003, Characterization of tectono-metamorphic events using crystal size distribution (CSD) diagram. A case study from the Acebuches metabasites (SW Spain): Journal of Structural Geology, 25(6), 935–947. https://doi.org/10.1016/S0191-8141(02)00081-0

Ennis, M.E., McSween, H.Y., 2014, Crystallization kinetics of olivine-phyric shergottites: Meteoritics and Planetary Science, 49(8), 1440–1455. https://doi.org/10.1111/MAPS.12349

Eskandari, A., Sadeghi, B., 2024, Deciphering

http://dx.doi.org/10.18268/BSGM2025v77n2a120325

Igneous Rock Crystals: Unveiling Multifractal Patterns in Crystal Size Dynamics: Minerals, 14(7), 660. https://doi.org/10.3390/MIN14070660/S1

Ferry, J.M., Watson, E.B., 2007, New thermodynamic models and revised calibrations for the Ti-in-zircon and Zr-in-rutile thermometers: Contributions to Mineralogy and Petrology, 154(4), 429–437. https://doi.org/10.1007/s00410-007-0201-0

Filiberto, J., Gross, J., Udry, A., Trela, J., Wittmann, A., Cannon, K.M., Penniston-Dorland, S., Ash, R., Hamilton, V.E., Meado, A.L., Carpenter, P., Jolliff, B., Ferré, E.C., 2018, Shergottite Northwest Africa 6963: A Pyroxene-Cumulate Martian Gabbro: Journal of Geophysical Research Planets, 123(7), 1823–1841. https://doi.org/10.1029/2018JE005635

Garrido, C.J., Kelemen, P.B., Hirth, G., 2001, Variation of cooling rate with depth in lower crust formed at an oceanic spreading ridge: Plagioclase crystal size distributions in gabbros from the Oman ophiolite: Geochemistry, Geophysics, Geosystems, 2(10). https://doi.org/10.1029/2000GC000136

Gómez-Rivera, F.J., 2019, Análisis petrológico e isotópico del Complejo Batolítico Aquila, suroccidente de México: México, Universidad Michoacana de San Nicolás de Hidalgo, tesis de maestría, 212 p.

Guevara-Alday, D.A., 2020, Petrogénesis Magmática del Ensamble Plutónico de Tumbiscatío, Michoacán: México, Universidad Michoacana de San Nicolás de Hidalgo, tesis de maestría.

Hamzah, W.N., Kurniawan, I.A., Abdurrachman, M., Sucipta, I.G.B.E., Suparka, M.E., 2018, Textural analysis and crystal size distribution of plagioclase from Ciremai's a'ā lava: Interpretation magmatic processes and crystallization time: IOP Conference Series: Earth and Environmental Science, 212(1), 012039. https://doi.org/10.1088/1755-1315/212/1/012039

Hernández-Bernal, M.S., Corona-Chávez, P., Trujillo-Hernández, N., Macías-Romo, C., Morán-Zenteno, D.J., Jiménez-Haro, A., Poli, S., 2021, The Cuitzeo granitic xenolith: evidence of an Early Miocene magma plumbing system in central Mexico: Revista Mexicana de Ciencias Geologicas, 38(1), 29–42. https://doi.org/10.22201/CGEO.20072902E.2021.1.1591

Hersum, T.G., Marsh, B.D., 2007, Igneous textures: On the kinetics behind the words. Elements: 3(4), 247–252. https://doi.org/10.2113/gselements.3.4.247

Higgins, M.D., 2000, Origin of megacrysts in granitoids by textural coarsening: A crystal size distribution (CSD) study of microcline in the Cathedral Peak Granodiorite, Sierra Nevada, California: Geological Society Special Publication, 168, 207–219. https://doi.org/10.1144/GSL.SP.1999.168.01.14

Higgins, M.D., 2006, Quantitative textural measurements in igneous and metamorphic petrology: UK, Cambridge University Press, 265 p. https://doi.org/10.1017/CBO9780511535574

Higgins, M.D., 2017, Quantitative investigation of felsic rock textures using cathodoluminescence images and other techniques: Lithos, 277, 259–268. https://doi.org/10.1016/j.lithos.2016.05.006

Holness, M.B., Morris, C., Vukmanovic, Z., Morgan, D.J., 2020, Insights Into Magma Chamber Processes From the Relationship Between Fabric and Grain Shape in Troctolitic Cumulates: Frontiers in Earth Science, 8, 1–18. https://doi.org/10.3389/feart.2020.00352

Hort, M., Spohn, T., 1991, Crystallization calculations for a binary melt cooling at constant rates of heat removal: implications for the crystallization of magma bodies: Earth and Planetary Science Letters, 107(3–4), 463–474. https://doi.org/10.1016/0012-821X(91)90093-W

Jerram, D.A., Higgins, M.D., 2007, 3D analysis

of rock textures: Quantifying igneous microstructures: Elements, 3(4), 239–245. https://doi.org/10.2113/gselements.3.4.239

Jerram, D.A., Martin, V.M., 2008, Understanding crystal populations and their significance through the magma plumbing system: Geological Society Special Publication, 304, 133–148. https://doi.org/10.1144/SP304.7

Jerram, D.A., Mock, A., Davis, G.R., Field, M., Brown, R.J., 2009, 3D crystal size distributions: A case study on quantifying olivine populations in kimberlites: Lithos, 112, 223–235. https://doi.org/10.1016/j.lithos.2009.05.042

Jerram, D.A., Davis, G.R., Mock, A., Charrier, A., Marsh, B.D., 2010, Quantifying 3D crystal populations, packing and layering in shallow intrusions: A case study from the Basement Sill, Dry Valleys, Antarctica: Geosphere, 6(5), 537–548. https://doi.org/10.1130/GES00538.1

Marsh, B.D., 1988, Crystal size distribution (CSD) in rocks and the kinetics and dynamics of crystallization - I. Theory: Contributions to Mineralogy and Petrology, 99(3), 277–291. https://doi.org/10.1007/BF00375362/METRICS

Marsh, B.D., 1998, On the interpretation of crystal size distributions in magmatic systems: Journal of Petrology, 39(4), 553–599. https://doi.org/10.1093/petroj/39.4.553

Marsh, B.D., 2013, On some fundamentals of igneous petrology: Contributions to Mineralogy and Petrology, 166(3), 665–690. https://doi.org/10.1007/s00410-013-0892-3

Martini, M., Ferrari, L., Lopez-Martinez, M., Cerca-Martinez, M., Valencia, V. Serrano-Duran, L., 2009, Cretaceous-Eocene magmatism and Laramide deformation in southwestern Mexico: No role for terrane accretion: Geological Society of America Memoirs, 204(07), 151–182. https://doi.org/10.1130/2009.1204(07)

Miller, C.F., McDowell, S.M., Mapes, R.W., 2003, Hot and cold granites: Implications of zircon saturation temperatures and preservation of inheritance: Geology, 31(6), 529–532. https://doi.org/10.1130/0091-7613(2003)031<0529:HACGIO>2.0.CO;2

Morán-Zenteno, D.J., Tolson, G., Martínez-Serrano, R.G., Martiny, B., Schaaf, P., Silva-Romo, G., Macías-Romo, C., Alba-Aldave, L., Hernández-Bernal, M.S., Solís-Pichardo, G.N., 1999, Tertiary arc-magmatism of the Sierra Madre del Sur, Mexico, and its transition to the volcanic activity of the Trans-Mexican Volcanic Belt: Journal of South American Earth Sciences, 12(6), 513–535. https://doi.org/10.1016/S0895-9811(99)00036-X

Morán-Zenteno, D.J., Martiny, B.M., Solari, L., Mori, L., Luna-González, L., González-Torres, E.A., 2018, Cenozoic magmatism of the Sierra Madre del Sur and tectonic truncation of the Pacific margin of southern Mexico: Earth-Science Reviews, 183, 85–114. https://doi.org/10.1016/j.earscirev.2017.01.010

Mutch, E.J.F., Blundy, J.D., Tattitch, B.C., Cooper, F.J., Brooker, R.A., 2016, An experimental study of amphibole stability in low-pressure granitic magmas and a revised Al-in-hornblende geobarometer: Contributions to Mineralogy and Petrology, 171(10), 85. https://doi.org/10.1007/s00410-016-1298-9

Ngonge, E.D., Archanjo, C.J., Hollanda, M.H.B.M., 2013, Plagioclase crystal size distribution in some tholeiitic mafic dykes in Cabo Frio-Buzios, Rio de Janeiro, Brazil: Journal of Volcanology and Geothermal Research, 255, 26–42. https://doi.org/10.1016/j.jvolgeores.2013.01.009

Nugroho, R.P., Disando, T., Kurniawan, I.A., Abdurrachman, M., 2019, Crystal size distribution (CSD) of plagioclase phenocryst-microphenocryst and the calculation of crystal resident times in the continuous

central eruption sequences of Mount Lasem, Central Java, Indonesia: Journal of Physics: Conference Series, 1363, 012041. https://doi.org/10.1088/1742-6596/1363/1/012041

Ortega-Gutiérrez, F., Elías-Herrera, M., Morán-Zenteno, D.J., Solari, L., Luna-González, L., Schaaf, P., 2014, A review of batholiths and other plutonic intrusions of Mexico: Gondwana Research, 26(3-4), 834–868. https://doi.org/10.1016/j.gr.2014.05.002

Rannou, E., Caroff, M., 2010, Crystal size distribution in magmatic rocks: Proposition of a synthetic theoretical model: Journal of Petrology, 51(5), 1087–1098. https://doi.org/10.1093/petrology/egq012

Resendiz-Zarco, E., 2024, Magmatismo del ensamble plutónico de San Diego Curucupatzeo, Michoacán: Geología, Petrología y Geoquímica: México, Universidad Michoacana de San Nicolás de Hidalgo, tesis de maestría.

Schaaf, P., Morán-Zenteno, D., Hernández-Bernal, M.S., Solís-Pichardo, G., Tolson, G., Köhler, H., 1995, Paleogene continental margin truncation in southwestern Mexico: Geochronological evidence: Tectonics, 14(6), 1339–1350. https://doi.org/10.1029/95TC01928

Shirzad, K., Viney, C., 2023, A critical review on applications of the Avrami equation beyond materials science: Journal of the Royal Society Interface, 20(203). https://doi.org/10.1098/rsif.2023.0242

Suazo-Cruz, G., 2020, Análisis geoquímico, geocronológico y estereológico de la porción NE del plutón paleógeno de Arteaga, Michoacán y su interpretación geológica: México, Escuela Nacional de Estudios Superiores, Unidad Morelia, Universidad Nacional Autónoma de México, tesis de licenciatura, 127 p.

Teran, A.V., Bergmann, R.B., Bill, A., 2010, Time-evolution of grain size distributions in random nucleation and growth crystallization processes: Physical Review B, 81, 075319. https://doi.org/10.1103/PhysRevB.81.075319

Villanueva-Lascuráin, D., Solís-Pichardo, G., Schaaf, P., Hernández-Treviño, T., Salazar-Juárez, J., Corona-Chávez, P., 2016, Age and origin of the gabbros in the Jilotlán pluton, Jalisco: Primitive magmatic rocks in the southern part of the Guerrero terrane: Revista Mexicana de Ciencias Geológicas, 33(1), 135–136. https://doi.org/10.22201/cgeo.20072902e.2016.1.646

Wang, D., Liu, J., Carranza, E.J.M., Zhai, D., Wang, Y., Zhen, S., Wang, J., Wang, J., Liu, Z., Zhang, F., 2019, Formation and evolution of snowball quartz phenocrysts in the Dongping porphyritic granite, Hebei Province, China: Insights from fluid inclusions, cathodoluminescence, trace elements, and crystal size distribution study: Lithos, 340–341, 239–254. https://doi.org/10.1016/J.LITHOS.2019.05.018

Yu, Y., Luo, B., Zhang, H., Xu, W., Yang, H., Pan, F., Guo, L., Li, J., Ruan, B., Lai, K., Zhang, Y., Cao, Z., 2023, Origin of K-feldspar megacrysts of Quxu batholith in Gangdese belt, South Tibet: Implication for magma rejuvenation in a crystal mush reservoir: Lithos, 438–439, 107019. https://doi.org/10.1016/j.lithos.2023.107019